

Home Search Collections Journals About Contact us My IOPscience

The mechanism for the nonlinear optical properties in ${\rm La_9Na_3B_8O_{27}}$, ${\rm La_2Na_3B_3O_9}$ and ${\rm La_2CaB_{10}O_{19}}$: ab initio studies

This content has been downloaded from IOPscience. Please scroll down to see the full text.

2015 J. Phys.: Condens. Matter 27 485501

(http://iopscience.iop.org/0953-8984/27/48/485501)

View the table of contents for this issue, or go to the journal homepage for more

Download details:

IP Address: 140.112.172.135

This content was downloaded on 29/12/2015 at 10:33

Please note that terms and conditions apply.

J. Phys.: Condens. Matter 27 (2015) 485501 (8pp)

doi:10.1088/0953-8984/27/48/485501

The mechanism for the nonlinear optical properties in La₉Na₃B₈O₂₇, La₂Na₃B₃O₉ and La₂CaB₁₀O₁₉: *ab initio* studies

Jia Zhang 1,3 , Lei Kang 1,3 , Tse-Hsing Lin 2 , Xingxing Jiang 1,3 , Pifu Gong 1,3 , Ming-Hsien Lee 2 and Zheshuai Lin 1

- ¹ Center for Crystal R&D, Key Lab of Functional Crystals and Laser Technology of Chinese Academy of Sciences, Technical Institute of Physics and Chemistry, CAS, Beijing 100190, People's Republic of China
- ² Department of Physics, Tamkang University, Tamsui, New Taipei 25137, Taiwan
- ³ University of Chinese Academy of Sciences, Beijing 100049, People's Republic of China

E-mail: zslin@mail.ipc.ac.cn and mhslee@mail.tku.edu.tw

Received 18 June 2015, revised 26 October 2015 Accepted for publication 28 October 2015 Published 16 November 2015



Abstract

The nonlinear optical (NLO) properties in $La_9Na_3B_8O_{27}$, $La_2Na_3B_3O_9$ and $La_2CaB_{10}O_{19}$ are investigated using a plane-wave pseudopotential method. Based on the first-principles electronic band structures, the birefringence and second harmonic generation (SHG) coefficients for the three crystals are determined. The calculated values match well with the experimental results. In order to elucidate the microscopic origins of the NLO performances in these crystals, a real-space atom-cutting method is adopted to calculate the contribution from the respective ions and groups. It is revealed that the La cations have covalent interactions with the neighbor O ions so as to form the La–O groups. The La–O bond covalency, combined with the distortion of La–O groups, makes the large contribution to the overall SHG coefficients in addition to the B–O groups, as also intuitively demonstrated by a SHG-density analysis.

Keywords: La-based borate crystals, nonlinear optical properties, first-principles calculations, structure—property relationship

1

(Some figures may appear in colour only in the online journal)

Introduction

In recent years the search of new nonlinear optical (NLO) materials in the ultraviolet (UV) spectral region, especially for the wavelength of 266 nm, has attracted intense attentions [1–5]. In particular, three new rare earth borate crystals were synthesized successfully: La₉Na₃B₈O₂₇ (L9NB) [6], La₂Na₃B₃O₉ (L2NB) [7] and La₂CaB₁₀O₁₉ (LCB) [8], which all contain the rare-earth element Lanthanum. Generally it is difficult for the short-wave absorption edges of the rare-earth compounds to reach the UV region where the wavelength is shorter than 300 nm because of the optical absorption from the d–d or f–f electronic transition. However, these unfavored transitions can be effectively inhibited in the rare-earth La³⁺ cations since their d electronic shells are fully-occupied (4d¹⁰). The energy band gaps for the three compounds are larger than 5.5 eV, i.e.

their UV absorption cutoffs are less than 230 nm [9–11]. Moreover, the second harmonic generation (SHG) effect in L9NB is about five times as strong as that of KDP ($\sim 0.39 \text{ pm V}^{-1}$) [6], while the SHG effects in L2NB and LCB are about twice as strong as that of KDP [7, 8]. Thus, these lanthanum borates are very promising NLO materials for producing second harmonic generation (SHG) in the UV spectral region, such as for the 266 nm laser. Interestingly, the NLO effects in these compounds are generally larger than those in the alkaline and alkaline earth borates which are commonly used to produce the UV coherent output, such as LiB₃O₅ [12], BaAlBO₃F₂ [13] and K₂Al₂B₂O₇ [14]. Therefore, it is very desirable to investigate the mechanism for the NLO responses in these three crystals. The understanding of structure-property relationship would greatly prompt the development of rare earth UV NLO borates.

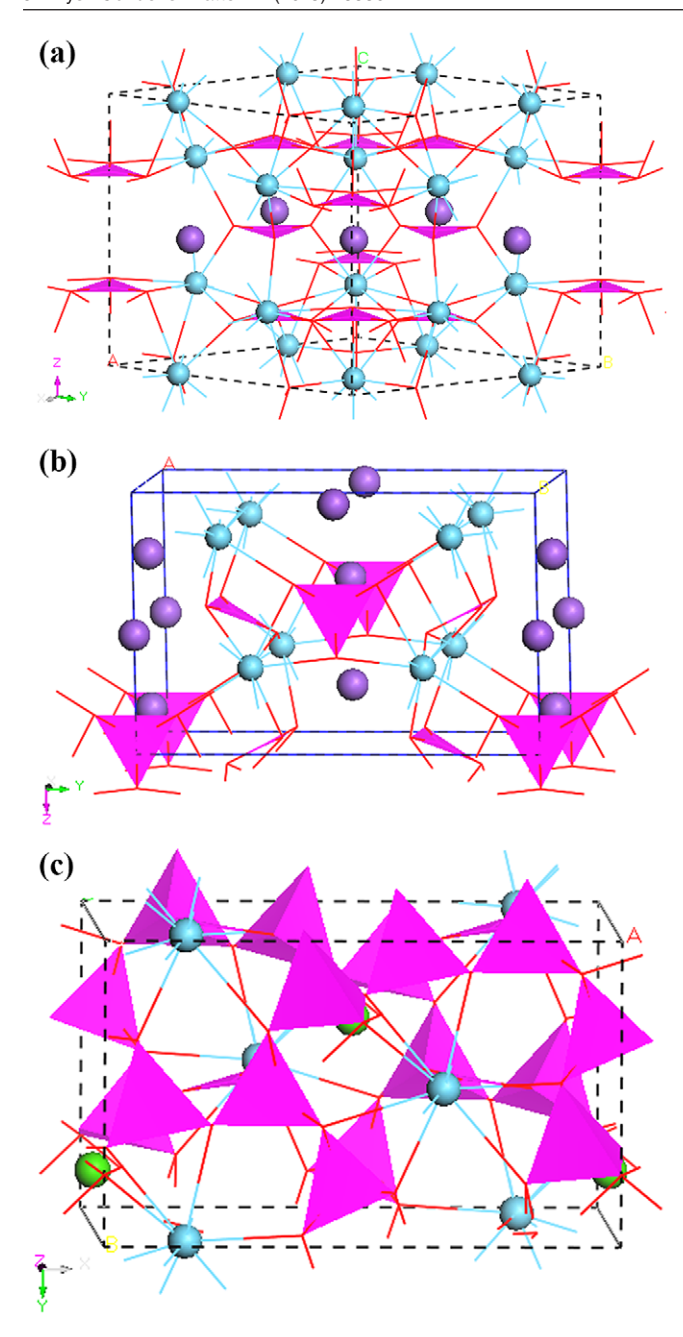


Figure 1. Unit cells for (a) L9NB, (b) L2NB, and (c) LCB. Violet, green and cyan balls are Na, Ca, and La atoms, respectively. The B–O groups are shown in magenta polyhedra; the $(BO_3)^{3-}$ groups in L9NB and L2NB, and the $(B_5O_{12})^{9-}$ groups in LCB.

The structures of L9NB, L2NB and LCB are displayed in figure 1. Their space groups are P62m, Amm2, and C2, respectively. In the three crystals, the basic building blocks are borate groups: $(BO_3)^{3-}$ anionic groups for L9NB and L2NB, and $(B_5O_{12})^{9-}$ anionic groups for LCB. In L9NB and L2NB the $(BO_3)^{3-}$ groups are isolated from each other [6, 7], while in LCB the $(B_5O_{12})^{9-}$ groups are linked together to form the infinite 2D double layers, which are almost perpendicular to the c-axis [8]. The La³⁺, Na⁺ or Ca²⁺ cations are located in the interstices. According to the anionic group theory proposed by Chen [15], the B–O groups are supposed to play a dominant role in producing the SHG effect in the UV borate crystals,

and the contribution from highly ionic cations, such as alkaline and alkaline earth cations (Na⁺ or Ca²⁺), is neglectably small. However, it is unclear whether this theory is still valid for the lanthanum borates, considering the relatively strong covalent characteristics of the La³⁺ cations. The clarification of this question is helpful for the understanding of the roles of rare earth elements in the NLO properties in these borate NLO crystals.

In this paper, we present the first-principles studies on the NLO properties in L9NB, L2NB and LCB. The electronic structures and NLO coefficients are calculated, which match well with the experimental results. Moreover, the real-space atom-cutting method and the SHG-density analysis have been adopted to investigate the respective contribution from the constituent ions (or groups) to the optical properties. It is demonstrated that the contributions from La–O groups to the NLO properties are comparable to those from the B–O groups in LCB, and even larger in L9NB and L2NB.

Computational methods

The electronic structures of the three crystals are calculated by the plane-wave pseudopotential method [16] implemented in the CASTEP package [17]. The exchange-correlation (XC) functional is described by the local density approximation (LDA) [18]. The core-electron interactions are modeled by the norm-conserving pseudopotentials [19] with the 1s electrons for B, O and Na, the 1s, 2s, and 2p electrons for Ca treated as core electrons. For La the 5d16s2 electrons are treated as valence electrons, in which the f orbitals are not included. It is because the f orbitals never form efficient covalent bond with oxygen s or p orbitals at close distance, and for larger distance, these orbitals again has poor overlap with oxygen since they are highly localized. Moreover, the relativistic treatment is applied on the La pseudopotentials [20, 21]. Kinetic energy cutoffs of 770eV for L9NB and L2NB and of 550eV for LCB, and Monkhorst–Pack k-point meshes [22] spanning less than 0.04 \mathring{A}^{-3} in the Brillouin zone are chosen to ensure the sufficient accuracy for the present purposes [23].

Based on the electronic band structures, the imaginary part of the dielectric function is calculated from the electronic transition between the occupied and unoccupied states caused by the interaction with photons [24]. The real part of the dielectric function is then determined using the Kramers–Kronig transform, from which the birefringence Δn are obtained. The birefringence is a key parameter to determine the phasematching condition for the NLO production in a crystal. Furthermore, the second order susceptibility $\chi^{(2)}$ and SHG coefficient d_{ij} ($d_{ij} = 1/2 \chi^{(2)}$) is calculated using an expression originally proposed by Rashkeev *et al* [25] and developed by Lin *et al* [26]:

$$\chi_{ijk} = \chi_{ijk}(VE) + \chi_{ijk}(VH) + \chi_{ijk}(two bands),$$

where χ_{ijk} (VE) and χ_{ijk} (VH) denote the contributions from virtual-electron processes and virtual-hole processes, respectively, and χ_{ijk} (two bands) gives the contribution from two band processes to $\chi^{(2)}$. In detail, the formulae for calculating χ_{ijk} (VE), χ_{ijk} (VH) and χ_{ijk} (two bands) are listed as following:

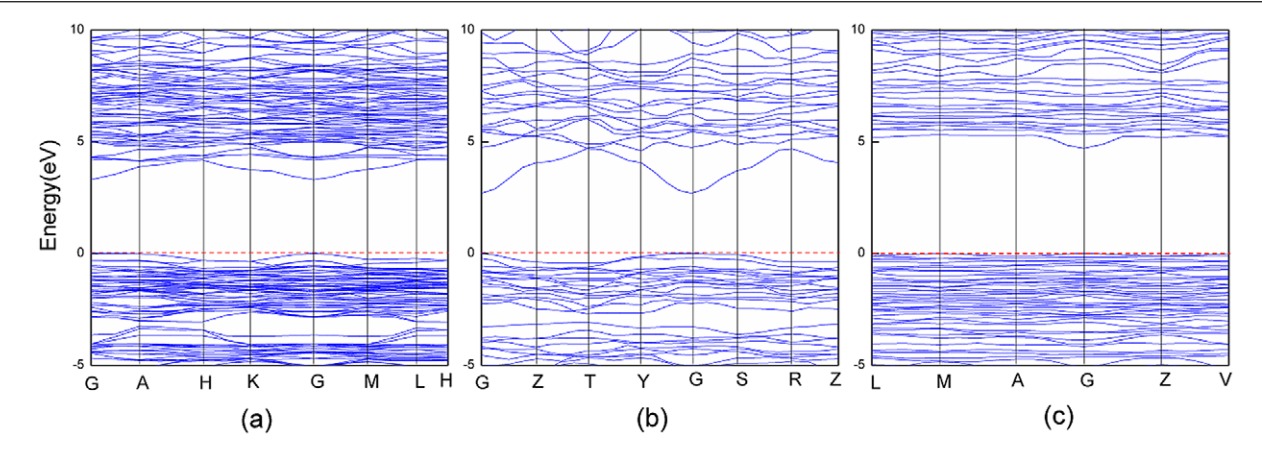


Figure 2. Electronic band structures for (a) L9NB, (b) L2NB and (c) LCB.

$$\begin{split} \chi_{ijk}(\text{VE}) &= \frac{e^3}{2\hbar^2 m^3} \sum_{vcc'} \int \frac{\mathrm{d}^3\vec{k}}{4\pi^3} P(ijk) \text{Im}[p_{vc}^i p_{cc'}^j p_{ct'}^k] \\ &\times \left(\frac{1}{\omega_{cv}^3 \omega_{vc'}^2} + \frac{2}{\omega_{vc}^4 \omega_{ctv}} \right) \\ \chi_{ijk}(\text{VH}) &= \frac{e^3}{2\hbar^2 m^3} \sum_{vv'c} \int \frac{\mathrm{d}^3\vec{k}}{4\pi^3} P(ijk) \text{Im}[p_{vv'}^i p_{vtc}^j p_{cv}^k] \\ &\times \left(\frac{1}{\omega_{cv}^3 \omega_{vtc}^2} + \frac{2}{\omega_{vc}^4 \omega_{cv'}} \right) \\ \chi_{ijk}(\text{two bands}) &= \frac{e^3}{\hbar^2 m^3} \\ &\sum_{vc} \int \frac{\mathrm{d}^3\vec{k}}{4\pi^3} P(ijk) \frac{\text{Im}[p_{vc}^i p_{cv}^j (p_{vv}^k - p_{cc}^k)]}{\omega_{vc}^5}. \end{split}$$

Here, i, j and k are Cartesian components, v and v' denote VB, and c and c' denote CB. P(ijk) denotes full permutation. It should be emphasized that the refractive indices and SHG coefficients can be accurately obtained by DFT in principle because these optical properties are determined by the virtual electronic excited processes which are described by the first-and second-order perturbations, respectively, on the ground state wavefunctions.

Based on the calculated d_{ij} , one can obtain the powder SHG effect $\langle d_{powder} \rangle$ by Kurtz–Perry method [27], i.e.:

$$\left\langle \left(d_{\text{powder}}^{2\omega}\right)^{2} \right\rangle = \frac{19}{105} \sum_{i} \left(d_{iii}^{2\omega}\right)^{2} + \frac{13}{105} \sum_{i \neq j} d_{iii}^{2\omega} d_{ijj}^{2\omega} + \frac{44}{105} \sum_{i \neq j} \left(d_{iij}^{2\omega}\right)^{2}$$
$$+ \frac{13}{105} \sum_{ijk,cyclic} d_{ijj}^{2\omega} d_{jkk}^{2\omega} + \frac{5}{7} \left(d_{ijk}^{2\omega}\right)^{2}.$$

In the $\langle d_{\rm powder} \rangle$ calculations, the particles for the simulation samples are assumed to be the same sizes as the measured ones. Thus, it is not necessary to consider the dependence of $\langle d_{\rm powder} \rangle$ on particle size.

In order to quantitatively identify the respective contribution from the constituent ions (or groups) to the overall NLO response, a real-space atom-cutting technique is employed [26]. Within this technique, the contribution of ion A to the nth-order susceptibility (denoted as $\chi^{(n)}(A)$) is obtained by cutting all ions except A from the original wave functions

Table 1. Comparison of the linear and nonlinear optical properties between scissors-corrected LDA and hybrid functionals (PBE0) method in L2NB crystal.

L2NB	Δn	d_{31}	d_{32}	d_{33}	$\langle d_{ m powder} \rangle$	
Exp.			0.67		$2 \times \text{KDP}$	
Cal. by LDA Cal. by PBE0		0.94 0.68	0.47 0.38	-0.44 -0.29	$1.9 \times \text{KDP}$ $1.3 \times \text{KDP}$	

 $\chi^{(n)}(A) = \chi^{(n)}(\text{all ions except } A \text{ are cut})$. Meanwhile, the SHG-density analysis [28, 29] is performed to give an intuitive visualization of the orbitals that contribute to the SHG effects in the real space. In this scheme, the considered SHG coefficient is 'resolved' onto each orbital or band, and then the SHG-weighted bands are used to sum the probability densities of all occupied (valence) or unoccupied (conduction) states. Thus, the quantum states irrelevant to SHG are not shown in the occupied or unoccupied 'SHG-densities', while the charge densities vital to SHG are highlighted in the real space.

Results and discussions

The electronic band structures along the symmetry lines in the Brillouin zones for L9NB, L2NB and LCB are plotted in figure 2. It is shown that L9NB and LCB have direct band gaps of 3.31 eV and 4.72 eV, respectively, while L2NB has an indirect band gap of 2.70 eV. These calculated values are smaller than the experimental data (5.53 eV for L9NB [9], 5.86 eV for L2NB [10] and 7.31 eV for LCB [11]). It is because LDA usually underestimates the energy band gap for wide-gap insulators due to the discontinuity of XC energy [30]. In order to calculate the optical coefficients, the scissors operator [31] is introduced to shift all the conduction bands (CB) up to match the experimental band gap. The scissorcorrected LDA method is simple, but this method can obtain the linear and nonlinear optical properties in good accuracy for the UV borate system [32]. It should be noted that although the hybrid functionals are much better than LDA for describing the XC interactions and more suitable for the band gap prediction, they introduce the non-local components into the Hamiltonian [33]. The addition of the non-local potential makes the commutator with the Hamiltonian extremely

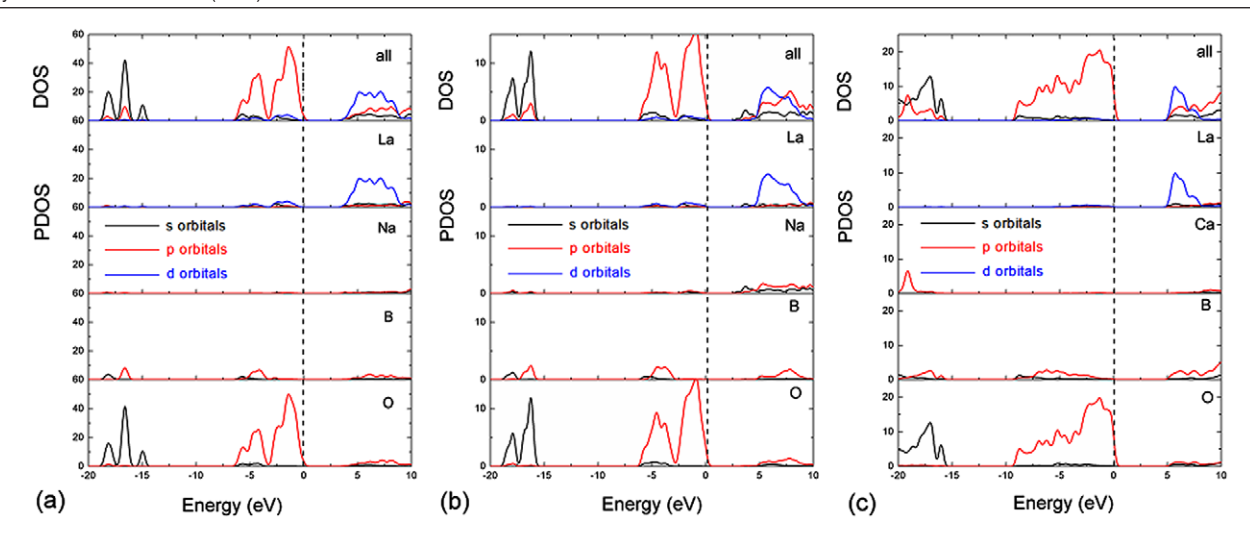


Figure 3. DOS and PDOS for (a) L9NB, (b) L2NB and (c) LCB. Black, red and blue curves represent s, p, d orbitals, respectively. Dashed straight lines indicate the VB maximum.

L9NB L2NB LCB Population Length (Å) Population Length (Å) Population Length (Å) Bond Bond Bond В-О 0.91 1.377 B-O 0.98 1.312 B-O 0.97 1.333 0.88 1.385 0.94 1.348 0.90 1.356 0.89 0.83 1.402 0.90 1.389 1.357 La-O 0.32 2.423 0.87 1.3880.81 1.373 0.21 2.455 La-O 0.21 2.437 0.57 - 0.761.382 - 1.5180.29 2.466 0.46 2.468 La-O 0.41 2.298 0.25 2.542 0.13 2.530 0.21 2.520 0.11 2.573 0.19 2.597 0.19 2.550 0.01 2.677 0.03 2.652 0.10 2.633 0.07 2.704 0.23 2.682 0.10 2.697

Table 2. Mulliken bond populations and bond lengths of L9NB, L2NB and LCB.

complex, thus breaks the usual expressions for transforming the optical matrix element from the position operator to the momentum operator, which might deteriorate the accuracy of optical property prediction. For a confirmation the comparison of optical properties calculated by scissor-corrected LDA and hybrid functionals in the studied crystals, for example, in L2NB, is shown in table 1. Of course, the scissors operators are usually determined by the difference between experimental and DFT bandgaps. However, our previous study demonstrated that the scissors operators can also be accurately determined by the difference between hybrid functionals (e.g. PBE0, B3LYP or sX-LDA) bandgaps and LDA bandgaps in the UV borate system [32]. This actually provides an *ab initio* path to predict the SHG properties without introducing any experimental data.

2.769

0.21

The total density of states (DOS) and the partial density of states (PDOS) projected on the constituent elements of the three crystals are displayed in figure 3, from which several common characteristics can be deduced: (i) The inner valence orbitals for the constituent ions (i.e. 2s orbitals for oxygen and boron, 2s and 2p orbitals for sodium, and 3s and 3p orbitals for calcium) are located at the deep region of the valence bands

(VB) below $-10\,\text{eV}$. These orbitals are quite localized, exhibiting the very weak interaction with other orbitals. (ii) The valence bands from $-10\,\text{eV}$ to $0\,\text{eV}$ are mainly composed of the 2p orbitals of oxygen and boron, but the O 2p orbitals have dominant contribution to the top of VB. The large hybridization between oxygen and boron orbitals indicates the formation of strong covalent bonds in the B-O groups. Moreover, the La 5d orbitals also have some contribution to the upper parts of the VB, and their hybridization with O 2p orbitals is clearly exhibited. This indicates that there exist covalent interactions between La³⁺ cations and O²⁻ anions. Similar conclusions can be deduced from the Mulliken population analysis as listed in table 2. It is clear that although the La–O bond populations are smaller than those on B-O bond, the reasonably covalent interactions between La and O are indeed presented in the three studied crystals. Meanwhile the La-O bond lengths are larger than the B-O bond lengths due to the larger size of the lanthanum cations. Normally, the larger La–O bond distance corresponds to the smaller covalency [34, 35]. However, under the restriction of symmetry some small bond lengths could also correspond to small covalency (e.g. in L2NB, a La-O bond length of 2.437 Å corresponds to the

0.07

0.04

2.669 2.779

Table 3. Comparison between the calculated (Cal.) and experimental (Exp.) birefringence Δn (@ 1064 nm), powder SHG effects $\langle d_{powder} \rangle$ (×KDP, d_{36} of KDP = 0.39 pm V⁻¹), and SHG coefficients d_{ij} (pm V⁻¹) for L9NB, L2NB and LCB. The real-space atom-cutting results are listed as well.

L9NB		Exp.	Cal.	Real-space atom-cutting results			
				(BO ₃) ³⁻	(La–O) ^a	Na ⁺	La ³⁺
	Δn	0.085	0.096	0.133	0.091	0.012	0.021
	$\langle d_{\mathrm{powder}} \rangle$	$(3-5) \times KDP$	$4 \times KDP$				
	d_{22}	2.31 [37]	2.23	1.19	1.93	0.08	0.17
L2NB				$(BO_3)^{3-}$	$(LaO_9)^{15-}$	Na ⁺	La^{3+}
	Δn	0.023	0.013	0.011	0.008	0.005	0.011
	$\langle d_{ m powder} \rangle$	$2 \times KDP$	$1.9 \times \text{KDP}$				
	d_{31}	1.45 [10]	-0.94	-0.47	-0.71	-0.02	0.02
	d_{32}	0.67	-0.47	-0.37	-0.38	0.01	0.07
	d_{33}	-1.06	0.44	-0.21	0.09	0.03	0.19
LCB				$(B_5O_{12})^{9-}$	$(LaO_{10})^{17-}$	Ca^{2+}	La^{3+}
	Δn	0.053	0.037	0.023	0.009	0.003	0.008
	$\langle d_{\mathrm{powder}} \rangle$	$2 \times KDP$	$1.1 \times KDP$				
	d_{14}	0.70	-0.08	-0.04	-0.13	0.01	-0.01
	d_{21}	0.58	0.58	0.46	0.19	0.01	0.06
	d_{22}	-1.04[11]	-0.69	-0.52	-0.44	-0.01	0.09
	d_{23}	0.25	-0.05	0.03	-0.02	~0	0.04

^aIncluding both (LaO₈)¹³⁻ groups and (LaO₉)¹⁵⁻ groups.

bond population of 0.21). This actually prompts the asymmetry of electronic distribution in the high-coordinated La-O polyhedra, and enhances the microscopic SHG response in these groups. (iii) The conduction band (CB) bottom is dominated by the 5d orbitals of lanthanum, with a quite large contribution from the 2p orbitals of boron and oxygen. The upper part of CB is composed of the orbitals of all constituent atoms. Since the optical properties of a crystal in the visible and UV regions are mainly determined by the electronic states close to the energy band gap [28, 36], it is expected that the B, O and La ions have major contribution to the optical birefringence and SHG effects in the three crystals. In addition, the PDOS diagrams of L9NB and L2NB are similar to each other, but are somewhat different from that of LCB. For L9NB and L2NB, the upper parts of VB of B and O are distributed from -6.5to 0 eV, while for LCB are from -9.5 to 0 eV. This is largely due to the different B-O building blocks: in L9NB and L2NB the building units are isolated (BO₃)³⁻ groups, while in LCB are (B₅O₁₂)⁹⁻ groups, which are linked together to form the infinite 2D double layers.

The birefringence Δn , PSHG effect $\langle d_{\text{powder}} \rangle$ and SHG coefficients d_{ij} for L9NB, L2NB and LCB are calculated and the results are listed in table 3, together with the available experimental data [10, 11, 37] for comparison. It is clear that the calculated values show a reasonable agreement with the experimental results, demonstrating the validity and accuracy of the first-principles method on the studied crystals. In order to further investigate the respective contribution of the constituent ions to the NLO responses, the atom-cutting technique is adopted. The cutting radii for B, O, La, Na, and Ca are set as 0.88 Å, 1.11 Å, 1.30 Å, 1.22 Å, and 1.26 Å, respectively, following the strategy presented in [26]. It is well known that the large covalent chemical bonds are formed between boron and oxygen ions, and the B–O groups need to be considered

as a whole. As a comparison, the sodium and calcium cations are strongly ionic and the surrounding charge densities are in spherical shape, so can be treated as isolated cations to be individually 'cut'. As for the lanthanum cations, since their interaction with the neighbor oxygen anions is reasonably covalent, as shown in the above electronic structure calculations, the La and O ions cannot be separately considered. In fact, if the La³⁺ cations are treated as isolated ions in the atom-cutting calculations, the sums of the SHG coefficients of B-O groups, Na⁺ (or Ca²⁺) cations and La³⁺ cations (see table 3) in the largest SHG tensors, d_{22} , d_{31} and d_{22} for L9NB, L2NB, and LCB are 1.44 pm V^{-1} , -0.47 pm V^{-1} , and -0.44 pm V^{-1} , respectively, which are significantly smaller than the original values 2.23 pm V^{-1} , -0.94 pm V^{-1} and -0.69 pm V^{-1} . Therefore, the interactions between the La³⁺ cations and the neighbor ions (i.e. O²⁻ anions) should not be ignored in the contribution to the overall SHG effects, and these ions must be considered as a whole in the atom-cutting calculations.

The real-space atom-cutting results for the birefringence and SHG coefficients in L9NB, L2NB and LCB are listed in table 3 as well, from which several conclusions can be summarized: (i) The contributions of the alkaline or alkaline earth cations (Na⁺ or Ca²⁺) to the optical properties, both birefringence and SHG effects, is negligibly small in the three crystals. This is also confirmed by the electronic structural analysis which shows few energy states of these cations near the energy band gap. (ii) The sum of the SHG coefficients from the respective B–O and La–O groups is larger than the original values, so is the birefringence. It is because the orbitals of the oxygen ions involved in these anionic groups are used twice in the real-space atom-cutting procedures. (iii) In the three crystals the anisotropy of the refractive indices, i.e. the birefringence, mainly comes from the strong

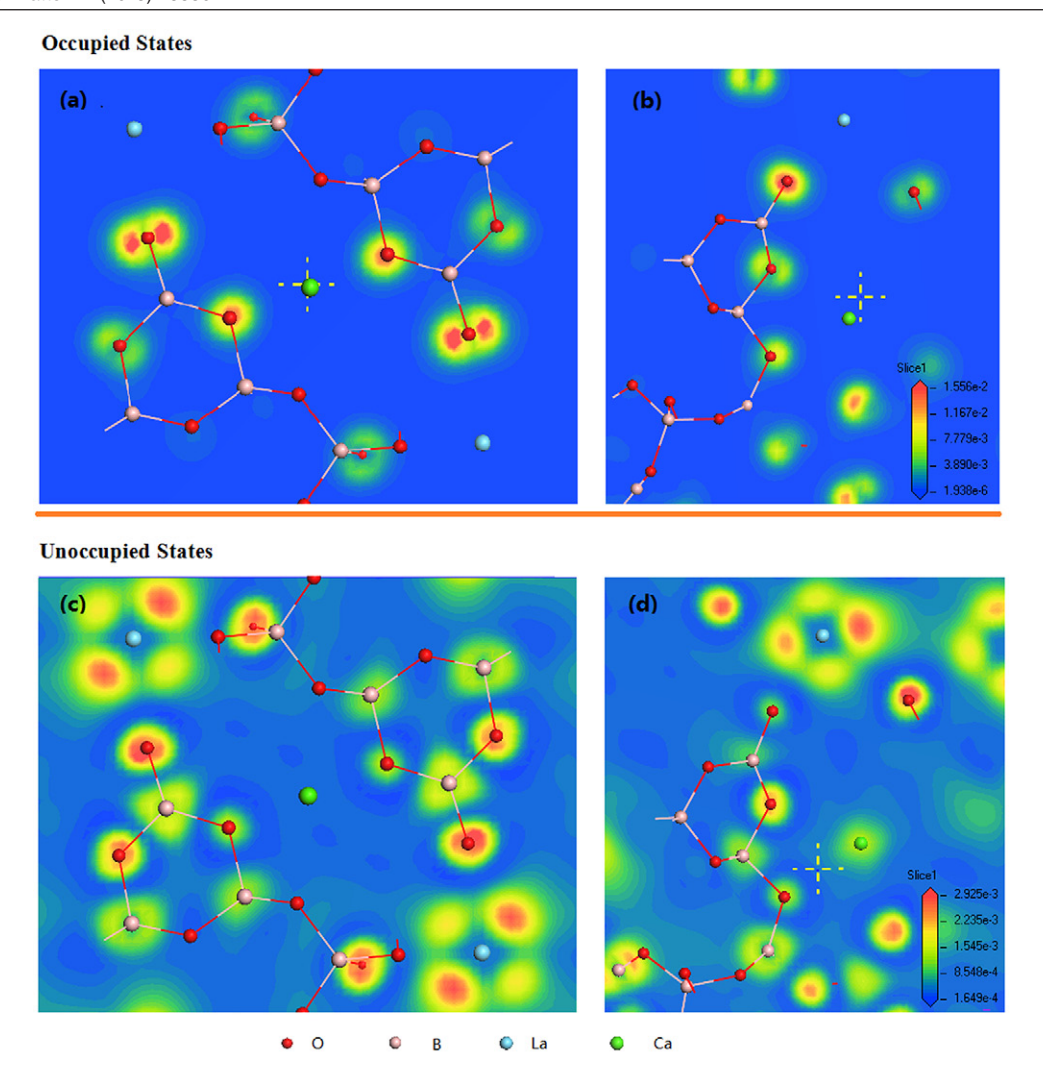


Figure 4. The SHG-density of the VE processes in LCB. (a) occupied states in a plane that contains La, B, and O ions. (b) occupied states in a plane containing La, Ca, B, and O ions. (c) unoccupied states in a plane containing La, B, and O ions. (d) unoccupied states in a plane containing La, Ca, B and O ions.

covalent $(BO_3)^{3-}$ or $(B_5O_{12})^{9-}$ groups. For the SHG effects, however, the contribution from the La–O groups is slightly larger than that from $(BO_3)^{3-}$ groups in L2NB and L9NB, while the La–O groups and the $(B_5O_{12})^{9-}$ groups have almost equal amounts of contribution in LCB.

Moreover, the SHG-densities of occupied and unoccupied states in LCB are displayed in figure 4 as a representative example. The SHG densities of occupied states (see figures 4(a) and (b)) show that the SHG weighted densities on the B-O groups (especially on O²⁻ anions) are dominant, while those on Ca²⁺ and La³⁺ cations are very small. For the unoccupied states (figures 4(c) and (d)) the nonspherical SHG densities accumulated on La cations are clearly exhibited: the distribution shapes indicate that these densities are mainly composed of the d orbitals on La cations. Meanwhile, there are also reasonably large SHG densities distributed within the areas of La-O groups and B-O groups. Unlike the La³⁺ cations, the orbitals around Ca²⁺ cations are spherical and relatively localized with lower density values (see figure 4(d)). All these results demonstrate that the B-O groups and La-O groups contribute dominantly to the overall SHG effects in LCB.

Similar to the situation in LCB, the SHG-densities are mainly distributed within the area of the La–O and B–O groups in L9NB and L2NB as well. Therefore, according to the SHG-density analysis of the title crystals, in addition to the B–O anionic groups, La³⁺ cations (and La–O groups) also play an important role in generating second harmonics, while the alkaline or alkaline earth cations make little contribution to the SHG effects. This is in accordance with the PDOS analysis (see figure 3) and the atom-cutting calculations (see table 3). In fact, these observations are also clearly exhibited in other rare earth NLO borates. For instance, in the crystal of YAl₃(BO₃)₄ [29] the contribution of (YO₆)^{9–} groups to the SHG coefficients is more than two times of that of (BO₃)^{3–} groups, while the contribution of Al³⁺ cations is negligibly small.

It should be noted that the SHG process is an effect which happens during electronic transition between occupied and empty states, so a spherical charge density as ground state may still be non-symmetrically polarizable. This is why one benefit from visualizing the unoccupied state SHG-density as well, which will show either direction-preferred charge

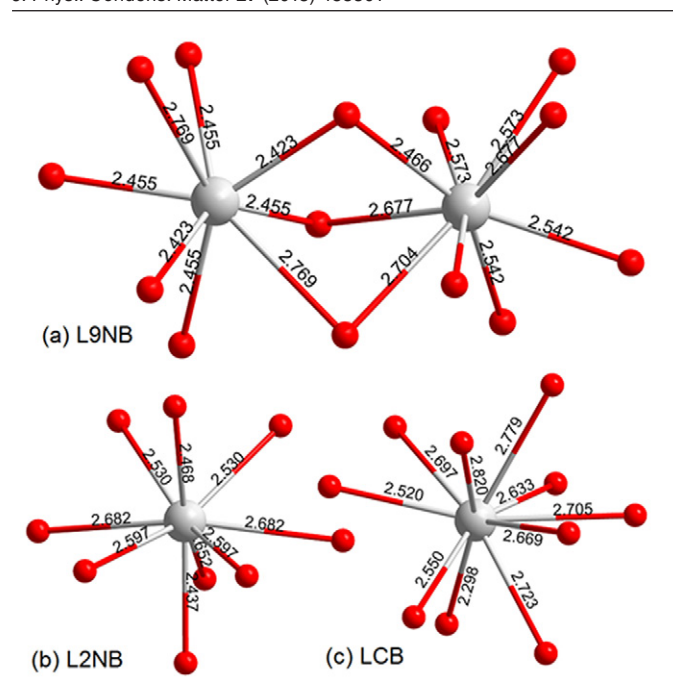


Figure 5. The La–O microscopic units in (a) L9NB, (b) L2NB and (c) LCB, respectively.

redistribution or charge-transfer excitation that could happen during the nonlinear charge response process. Unlike model calculations, our atomistic-realistic Kohn—Sham Hamiltonians do not assume reflection symmetry, i.e. parity is therefore not a good quantum number for its solution. It is not possible and unnecessary to specify parity in any Kohn—Sham orbital.

The structure–property relation analysis shows that the La³⁺ cations are chemically bonded to the neighbor oxygen ions. Figure 5 clearly shows that La–O polyhedral are strongly distorted. This structural feature, combined with the covalent chemical bonds, makes the La–O groups have large SHG responses which are comparable to or even larger than that of the B–O groups. It is noteworthy that in L9NB the $(BO_3)^{3-}$ groups are all arranged parallel to the a–b plane (although the orientation of one quarter of the $(BO_3)^{3-}$ groups is in opposite direction), and the geometrical superposition of the distortion of all $(LaO_8)^{13-}$ and $(LaO_9)^{15-}$ groups is largely along the b-axis (or the y-axis). As a comparison, in L2NB and LCB the B–O groups are located along the inclined directions. Therefore, the SHG coefficient (d_{22}) in L9NB is much larger than the values in L2NB and LCB.

Conclusions

The UV NLO lanthanum borates La₉Na₃B₈O₂₇, La₂Na₃B₃O₉ and La₂CaB₁₀O₁₉ are theoretically studied, with the purpose of investigating their microscopic mechanism of the optical responses. The electronic structures, birefringence and SHG coefficients of the three crystals are determined by the first-principles calculations based on the plane-wave pseudopotential method. The calculated results are in reasonable agreement with the experimental data. The SHG-density analysis demonstrates that orbitals of B, O and La ions are

the main origins of SHG. A real-space atom-cutting analysis reveals that in the three crystals the contribution of the La–O groups to SHG effects are comparable to or larger than that of the B–O groups: the interactions between La and O ions, as well as the La–O distorted groups, are significantly responsible for the optical nonlinearity. The combined contribution of La–O and B–O anionic groups results in the relatively large SHG effects in the crystals. We believe that these understandings of the microscopic mechanism of the NLO properties in the three lanthanum borate crystals are beneficial for the research and design of new rare earth borate NLO materials.

Acknowledgments

This work was supported by the NSF of China (Grants 11174297 and 11474292), China '863' projects (Grant 2015AA034203), and the Special Foundation of the Director of Technical Institute of Physics and Chemistry, CAS.

References

- [1] Zhao S, Gong P, Bai L, Xu X, Zhang S, Sun Z, Lin Z, Hong M, Chen C and Luo J 2014 Nat. Commun. 5 4019
- [2] Zhao S, Gong P, Luo S, Bai L, Lin Z, Ji C, Chen T, Hong M and Luo J 2014 *J. Am. Chem. Soc.* **136** 8560
- [3] Zhao S, Gong P, Luo S, Liu S, Li L, Asghar M A, Khan T, Hong M, Lin Z and Luo J 2015 J. Am. Chem. Soc. 137 2207
- [4] Kang L, Luo S, Huang H, Ye N, Lin Z, Qin J and Chen C 2013 J. Phys. Chem. C 117 25684
- [5] Zhao S, Zhang J, Zhang S Q, Sun Z, Lin Z, Wu Y, Hong M and Luo J 2014 *Inorg. Chem.* **53** 2521
- [6] Zhang G, Wu Y, Li Y, Chang F, Pan S, Fu P and Chen C 2005 J. Cryst. Growth 275 E1997
- [7] Zhang G C, Wu Y C, Fu P Z, Wang G F, Pan S L and Chen C T 2001 Chem. Lett. 5 456
- [8] Wu Y C, Liu J G, Fu P Z, Wang J X, Zhou H Y, Wang G F and Chen C T 2001 Chem. Mater. 13 753
- [9] Li Y G, Wu Y C, Zhang G C, Fu P Z and Bai X Y 2006 J. Cryst. Growth 292 468
- [10] Li K, Zhang G, Guo S, Zhang X, He R, Zhang J, Lin Z and Wu Y 2013 Opt. Laser Technol. 54 407
- [11] Zhang J X, Wang L R, Wu Y, Wang G L, Fu P Z and Wu Y C 2011 Opt. Express 19 16722
- [12] Lin S J, Sun Z Y, Wu B C and Chen C T 1990 *J. Appl. Phys.* 67 634
- [13] Hu Z G, Yoshimura M, Mori Y and Sasaki T 2004 J. Cryst. Growth 260 287
- [14] Ye N, Zeng W R, Jiang J, Wu B C, Chen C T, Feng B H and Zhang X L 2000 *J. Opt. Soc. Am.* B **17** 764
- [15] Chen C T et al 2012 Nonlinear Optical Borate Crystals (Germany: Wiley-VCH)
- [16] Milman V, Winkler B, White J A, Pickard C J, Payne M C, Akhmatskaya E V and Nobes R H 2000 Int. J. Quant. Chem. 77 895
- [17] Clark S J, Segall M D, Pickard C J, Hasnip P J, Probert M J, Refson K and Payne M C 2005 Z. Kristallogr. 220 567
- [18] Kohn W and Sham L J 1965 Phys. Rev. 140 1133
- [19] Kresse G and Joubert D 1999 Phys. Rev. B 59 1758
- [20] Sastri V R, Perumaraeddi J R, Rao V R, Rayudu G and Bunzli J 2003 Modern Aspects of Rare Earths and their Complexes (Amsterdam: Elsevier)

- [21] Pickard C J, Winkler B, Chen R K, Payne M C, Lee M H, Lin J S, White J A, Milman V and Vanderbilt D 2000 Phys. Rev. Lett. 85 5122
- [22] Monkhorst H J and Pack J D 1976 Phys. Rev. B 13 5188
- [23] Lin Z, Jiang X, Kang L, Gong P, Luo S and Lee M-H 2014 J. Phys. D: Appl. Phys. 47 253001
- [24] Palik E D 1985 Handbook of Optical Constants of Solids (New York: Academic)
- [25] Rashkeev S N, Lambrecht W R L and Segall B 1998 Phys. Rev. B 57 3905
- [26] Lin J, Lee M H, Liu Z P, Chen C T and Pickard C J 1999 Phys. Rev. B 60 13380
- [27] Kurtz S K and Perry T T 1968 J. Appl. Phys. 39 3798
- [28] Lee M H, Yang C H and Jan J H 2004 *Phys. Rev.* B **70** 235110

- [29] He R, Lin Z S, Lee M H and Chen C T 2011 J. Appl. Phys. 109 103510
- [30] Wang C S and Klein B M 1981 Phys. Rev. B 24 3417
- [31] Godby R W, Schluter M and Sham L J 1988 *Phys. Rev.* B **37** 10159
- [32] Lin Z S, Kang L, Zheng T, He R, Huang H and Chen C T 2012 Comput. Mat. Sci. 60 99
- [33] Asahi R, Mannstadt W and Freeman A 1999 *Phys. Rev.* B **59** 7486
- [34] Mulliken R S 1955 J. Chem. Phys. 23 1833
- [35] Cammarata A, Zhang W G, Halasyamani P S and Rondinelli J M 2014 *Chem. Mater.* **26** 5773
- [36] Lo C-H 2005 Master Degree Thesis Tamkang University
- [37] Zhang J X, Wang G L, Liu Z L, Wang L R, Zhang G C, Zhang X, Wu Y, Fu P Z and Wu Y C 2010 *Opt. Express* **18** 237